Desalination and Water Treatment
www.deswater.com

doi: 10.1080/19443994.2016.1172514

57 (2016) 27627–27637
December

Taylor & Francis
Taylor & Francis Group

Adsorption of methylene blue by porous ceramics prepared from electrolytic manganese residues

Fang-Fang Wu, Shuai Wang*, Shuai-Yi Guo, Hong Zhong*

College of Chemistry and Chemical Engineering, Central South University, Changsha 410083, China, Tel. +86 13975877503; email: wufangfang198732@163.com (F.-F. Wu), Tel. +86 731 88879616; email: wangshuai@csu.edu.cn (S. Wang), Tel. +86 18207417944; email: 383340944@qq.com (S.-Y. Guo), Tel. +86 731 88879616; email: zhongh@csu.edu.cn (H. Zhong)

Received 14 October 2015; Accepted 27 March 2016

ABSTRACT

The present work developed and analyzed an appropriate conversion method for electrolytic manganese residues (EMR) into a porous ceramics adsorbent for methylene blue (MB), which is simple in preparation and regeneration process, low in price, convenient in separation process, good reproducibility and environmentally friendly. The physicochemical properties of the electrolytic manganese residue-based porous ceramics (EMR-based ceramics) were characterized by X-ray diffraction, scanning electron microscopy, FT-IR, BET specific surface area, and BJH pore size distribution measurement. The effects of the contact time, temperature, initial concentration of MB, and pH on the adsorption process were studied. The kinetics, isotherm, thermodynamics, and mechanism analysis were investigated in detail. The results showed that the adsorption kinetics suitability used the pseudo-second-order kinetic model, and the adsorption isotherm data were fitted well to the Freundlich isotherm model. The thermodynamic parameters indicated that the adsorption process was a spontaneous, endothermic, and entropic-adding process. In conclusion, the EMR-based porous ceramics could be utilized as an adsorbent for the removal of MB effectively and repeatedly.

Keywords: Adsorption; Porous ceramics; Electrolytic manganese residues; Methylene blue

1. Introduction

Dyes are widely used in various industries to color their product, such as textiles, plastics, paper-making, foods, leather, cosmetics, pharmaceuticals, and others. The discharge of such colored effluents deteriorates the water quality and thus inhibits the growth of aquatic plants. Furthermore, this contamination of drinking water by dyes at even a concentration of 1.0 mg/L could cause harm to human health. Most of these dyes are characterized by stability because of their complex aromatic structures, which are difficult to photodegrade, biodegrade, and oxidize [1]. Water contamination that is caused by dyes has become a current environmental issue all over the world [2]. Methylene blue (MB), as a thiazine cationic dye, has wide application in hair colorants, paper making, and cotton coloring. Although MB is less hazardous, it can cause some harmful effects on humans such as shock, eye burns, rapid heartbeat, dyspnea, vomiting, jaundice, cyanosis, and tissue necrosis [3]. In the past few years, various techniques have been used for the

*Corresponding authors.

removal of MB, such as adsorption [4,5], photodecomposition [6], and catalytic degradation [7]. Among these, adsorption has been vastly reported because of its flexibility, simplicity of design, high efficiency, and ability to separate a wide range of chemical compounds [8].

Recently, considering the source abundance, engineering convenience, cost and removal efficiencies for large-scale utilization, much attention have been paid to the preparation of adsorbents using industrial byproducts or plant waste materials [9]. Many electrolytic manganese residues (EMR) are produced from the electrolytic manganese metal (EMM) industry as the main solid waste. In China, to produce 1 ton of EMM, approximately 6–9 tons of EMR are discharged into the environment [10]. The situation has become worse with the gradual degradation of manganese ores due to the depletion of high-grade manganese mineral resources, which means more and more EMR will be generated. EMR are an extremely hazardous environmental pollutant whose negative impact is profoundly studied [11]. The harmless disposal and resource utilization of EMR has become a hot topic of research around the world from the viewpoint of electrolysis manganese industries and environmental protection.

As an EMM industry byproduct, EMR mainly contain valuable mineral resources such as SiO_2, Al_2O_3, and other oxides. The chemical compositions of EMR make them suitable for use as the raw material for aluminosilicate-based porous ceramics. Porous ceramics have attained increasing attention for their wide range of engineering application because of their high porosity, moderate surface area, and excellent acidity and alkali resistance, and some applications include separation membranes [12], filters [13], piezoelectric [14] and pyroelectric ceramics [15], lightweight structural materials [16], biomaterials [17], battery separators [18], and solid oxide fuel cell electrodes [19]. In addition, although EMR contain some heavy metals, it was proven that heavy metals could be immobilized during the process of high-temperature sintering in the production process of the ceramics [20,21]. That is, ceramic production using EMR as the raw material could be one of the most favorable solutions for treating them. Furthermore, most adsorbents applied in wastewater treatment are characterized as fine particles or powders that would be suspended in wastewater, resulting in difficulties in their separation or even blocking flumes. Ceramics are suitable candidates for adsorbents because of their convenient separation. Therefore, electrolytic manganese residue-based porous ceramics (EMR-based ceramics) are nonhazardous and valuable adsorbents showing promising potential application in environmental protection.

This work prepared EMR-based porous ceramics for application in MB adsorption. The effects of contact time, temperature, initial MB concentration, and pH on the adsorption properties of MB were investigated in detail. The data were also explained on the basis of kinetic and thermodynamic models.

2. Experiments

2.1. Materials and characterizations

EMR were obtained from the western part of Hunan Province, China. The chemical compositions of EMR are listed in Table 1. The residues mainly consist of SiO_2, Al_2O_3, MnO, CaO, and Fe_2O_3. Phase analysis of the EMR was also characterized by X-ray diffraction (XRD) and scanning electron microscopy (SEM), as shown in Figs. 1 and 2, respectively. Fig. 2 shows that the EMR were amorphous laminated structures with some crystalline phase dispersing in the interstices of the large particles, ultimately forming a dense structure, which is beneficial to molding and sintering.

The additives used in the preparation of ceramics were as follows: (1) starch-Sunlight Food Co., food grade, (2) carbon powder, (3) dolomite—69.23 wt% $CaCO_3$ and 27.30 wt% $MgCO_3$, and (4) kaoline—46.31 wt% SiO_2 and 36.23 wt% Al_2O_3. Samples of EMR, carbon powder, dolomite, and kaoline were prepared after crushing, milling, and sieving to a +160 mesh.

MB was purchased from Tianjing Chemical Reagent Research Institute, China. All chemicals and reagents used in the experiments were of analytical grade and used without further purification.

2.2. Preparation of EMR-based porous ceramics

The EMR were washed three consecutive times as pre-treatment. The EMR (0.75 g) were then mixed with a mixture of 0.05 g kaoline, 0.2 g carbon powder, 0.075 g dolomite, and 0.1 ml deionized water in a beaker and molded in cylinder with a size of 10 × 5 mm under 3 MPa pressure for 3 min. The specimens rested overnight to allow the water to distribute evenly and were then fed into a furnace sintering in air at 1,100˚C for 1 h. The heating rate is shown in Fig. 3.

2.3. Adsorption experiments

A stock solution of MB (1,000 mol L^{-1}) was prepared and diluted to desired concentrations of 20, 50 100, 150 200, 300, 500, and 1,000 mol L^{-1}. The batch adsorption experiments were conducted in 50-ml conical flasks with 25 ml of standard solutions to

Table 1
Chemical compositions of the EMR

Compositions	MnO	Fe_2O_3	SiO_2	Al_2O_3	CaO	MgO	K_2O	Na_2O	TiO_2
Contents (wt%)	10.90	7.87	24.60	12.15	8.59	1.71	2.43	2.70	0.41

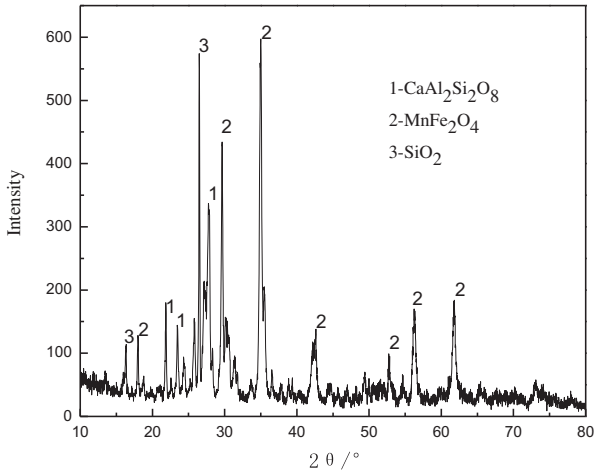

Fig. 1. XRD pattern of the EMR.

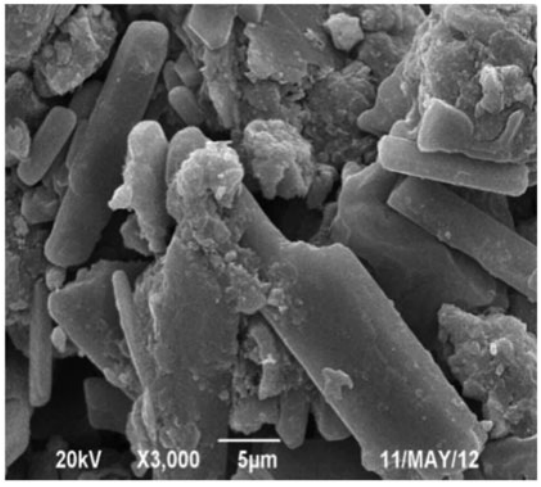

Fig. 2. SEM image of the EMR.

investigate the effects of the contact time, temperature, initial MB concentration, and pH on the adsorption properties of MB. In each experiment, one porous ceramic (approximately 0.5 g) was added to the dye solution, and the pH was adjusted using 0.1 mol L^{-1} NaOH solution and 0.1 mol L^{-1} HCl solution. The solution was then placed in a temperature-controlled water bath shaker at temperatures of 30, 40, and 50°C

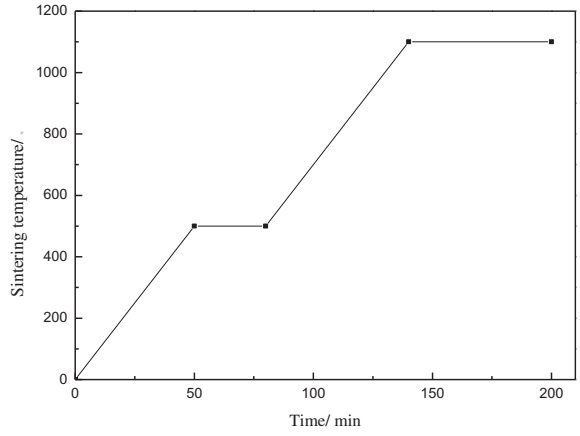

Fig. 3. Heating curves in the preparation process of the ceramics.

for a certain time. At the end of the experiments, the EMR-based ceramics were removed using a tiny pair of tweezers, and the remaining concentration of MB in the solution was determined at a characteristic wavelength of 664 nm by a UV–visible spectrophotometer. The adsorption capacity and removal ratio of MB were calculated according to the following equations:

$$q_t = \left(\frac{c_0 - c_t}{m}\right) V \quad (1)$$

$$R\% = \frac{c_0 - c_t}{c_0} \times 100 \quad (2)$$

where q_t (mg g^{-1}) is the adsorption capacity of MB at any time t (min). c_0 and c_t (mol L^{-1}) are the initial and final concentrations of MB, respectively, V (L) is the volume of the solution, and m (g) is the weight of the adsorbent.

3. Results and discussions

3.1. Characterization of EMR-based porous ceramics

EMR-based porous ceramics were characterized by XRD, SEM, pore size distribution, and FT-IR. The XRD results show that there are four phases in the ceramic materials: jacobsite ($MnFe_2O_4$), anorthite ($CaAl_2Si_2O_8$),

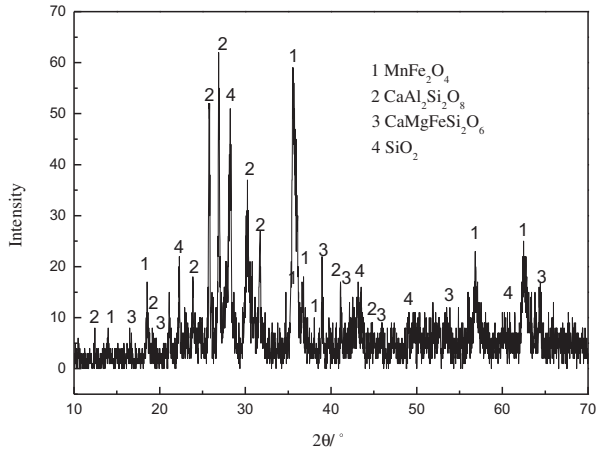

Fig. 4. XRD pattern of the EMR-based porous ceramics.

quartz (SiO_2), and pyroxene ($CaMgFeSi_2O_6$), as shown in Fig. 4, which means that the immobilization of manganese has been effectively achieved in the productive process of EMR-based porous ceramics. Therefore, the EMR-based ceramics are environmentally friendly adsorbents.

The comprehensive performance of the EMR-based porous ceramics is shown in Table 2. It was obvious that EMR-based porous ceramics have high compressive strength and apparent porosity, moderate surface area, and excellent acidity and alkali resistance, which makes them advantageous to use as an adsorbent to remove pollutants in wastewater.

Fig. 5 shows the SEM images of EMR-based porous ceramics before and after adsorption. It can be seen that EMR-based porous ceramics before adsorption presented a heterogeneous, rough, and relatively porous surface that can facilitate solution diffusion through the pores of the ceramics. From an adsorption viewpoint, more amorphous structures are desirable because more adsorption sites are available for adsorbate binding [22,23]. Moreover, based on the results of the BJH pore size distribution (shown in Fig. 6), most of the pores fall within the range of a mesoporous structure according to the IUPAC pore size classification [24]. It can also be observed that the type of the nitrogen adsorption isotherm is associated with a type II isotherm according to IUPAC classification. This isotherm suggests the typical characteristics of mesoporous and macroporous materials [25]. The cumulative pore volume and average pore size for EMR-based porous ceramics were 0.005 cc g^{-1} and 3.433 nm, respectively. The molecule size of MB is 1.382 nm, and thus, the mesoporous EMR-based porous ceramics are capable of effectively adsorbing MB molecules.

The FT-IR spectra of the EMR-based porous ceramics before and after adsorption are depicted in Fig. 7. The main intense bands for EMR-based porous ceramics before adsorption were observed at 1,144, 922, 669, and 592 cm^{-1}. After the adsorption of MB onto the ceramics, many functional groups shifted to different bands or appeared. The band at 1,144 cm^{-1} slightly transferred to lower frequency band at 1,141 cm^{-1}, whereas the peak at 669 cm^{-1} shifted to a higher frequency band at 677 cm^{-1}. Moreover, peaks at 3,165 and 1,420 cm^{-1} appeared after adsorption. The broadband centered at 3,165 cm^{-1} was related to N–H stretching. The band at 1,420 cm^{-1} was associated with the existence of aromatic rings. The shift and appearance of different peaks on the EMR-based porous ceramics after adsorption indicated the possible interaction of surface sites with MB, which can be taken as a sign of the effective adsorption of MB to the EMR-based porous ceramics.

3.2. Effects of temperature and contact time

The effects of the temperature and contact time on MB adsorption were investigated using an initial MB concentration of 50 mg L^{-1} and a pH of 9. The results are presented in Fig. 8. The figure shows that the adsorption of MB increased rapidly at the initial stage, where approximately 90% saturation was attained within 180 min, and as the amount of time increased, the adsorption rate decreased considerably. Subsequently, equilibrium was reached at 360 min. It can also be found that higher temperature resulted in an increase in the adsorption capacity of MB, suggesting that the adsorption of MB was endothermic in nature and that the adsorption process appeared to be chemisorption.

Table 2
The comprehensive performance of EMR-based porous ceramics

Compressive strength (MPa)	Apparent porosity (%)	Water absorption (%)	Bulk density (g cm^{-3})	Acidity resistant (%)	Alkali resistant (%)	Specific surface area (m^2 g^{-1})
6.97	69.70	71.40	0.97	90.26	97.94	0.897

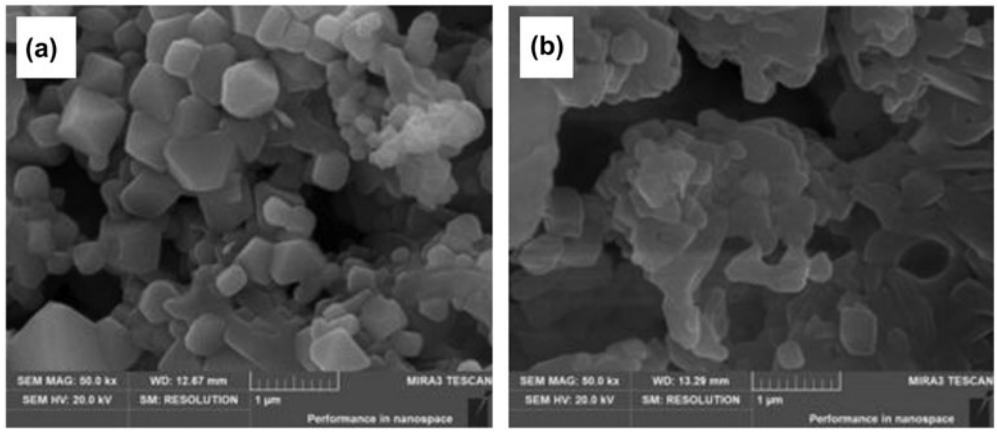

Fig. 5. SEM images of EMR-based porous ceramics (a) before and (b) after adsorption.

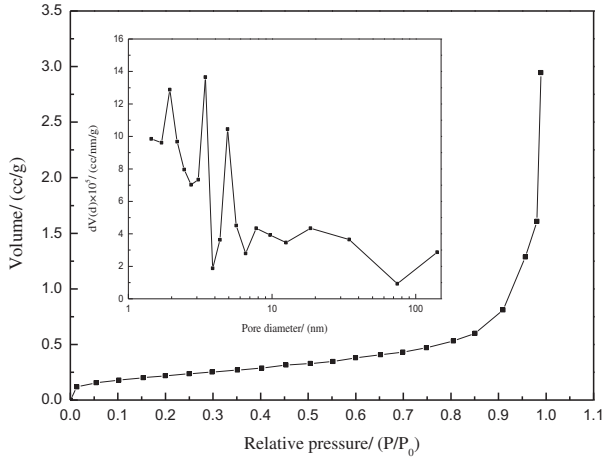

Fig. 6. The BET analysis and BJH pore size distribution of the EMR-based porous ceramics.

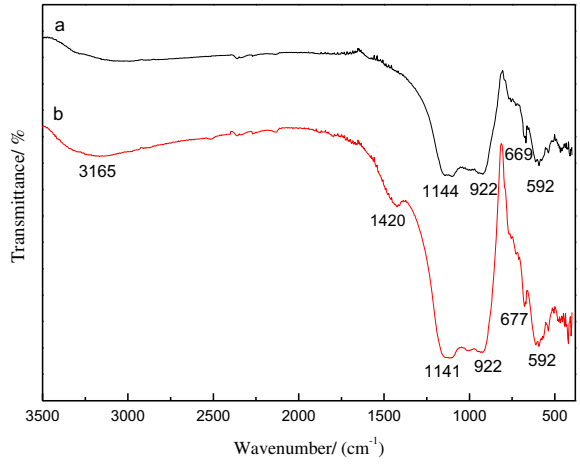

Fig. 7. The FT-IR spectra of the EMR-based porous ceramics (a) before and (b) after adsorption.

3.3. Effect of the initial concentration of MB

The effect of the initial concentration of MB on MB adsorption is depicted in Fig. 9. The figure shows that the adsorption capacity of MB greatly increased with an increase in the initial concentration of MB. In addition, the increase in the initial concentration of MB from 20 to 1,000 mg L^{-1} increased the adsorption capacity of MB by more than 32 times at a temperature of 50°C. The superior adsorption capacity of MB at a high initial concentration may be due to the significant driving forces that are caused by the concentration gradient [26]. Moreover, the external and internal mass transfer mechanisms are also favored [27,28]. Similar results were obtained about the effect of the initial MB concentration on the adsorption capacity [29]. The results also indicated that it was suitable for a wide range of initial MB concentration wastewater treatments.

3.4. Effect of pH

The effect of pH on the adsorption capacity of MB on EMR-based porous ceramics was evaluated using a temperature of 50°C, an initial concentration of 50 mg L^{-1}, and a contact time of 360 min with pH values from 2 to 12. The results are shown in Fig. 10.

It was obvious that the adsorption capacity and removal ratio of MB increased as the pH value increased from 2 to 12. This occurred because EMR-based porous ceramics are negatively charged at higher pH values, whereas the MB molecules mainly exist in the form of a cationic form. Thus, the pH

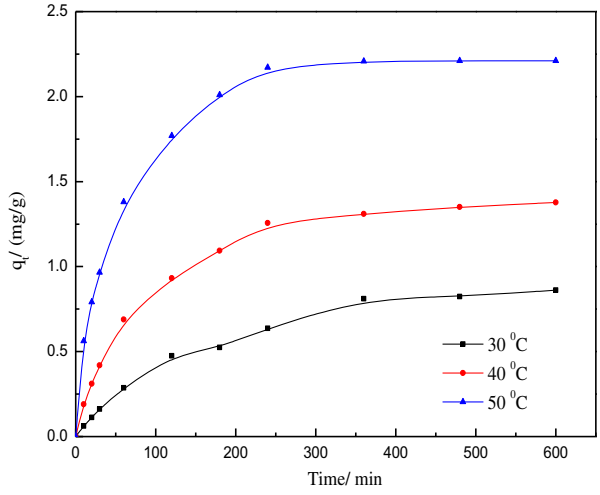

Fig. 8. The effects of the temperature and contact time on MB adsorption.

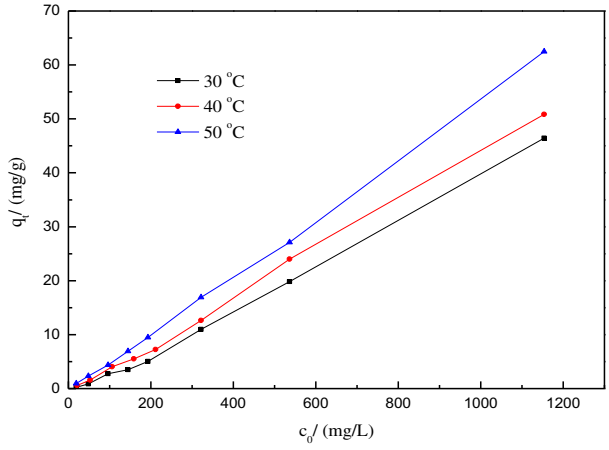

Fig. 9. The effect of the initial concentration of MB on MB adsorption.

increase facilitates the interaction between the negatively charged ceramics with the cationic MB. At lower pH values, the lower adsorption capacity and removal ratio of MB can be attributed to the competition of hydrogen ions with the MB molecules in the cationic form and the repulsive force between the positively charged ceramics and MB [30].

3.5. Kinetics of MB adsorption

To examine the adsorption kinetic behavior of the EMR-based ceramics, the kinetic data in Fig. 8 were applied to pseudo-first-order and pseudo-second-order kinetic models. The linear forms of these two kinetic models can be expressed as:

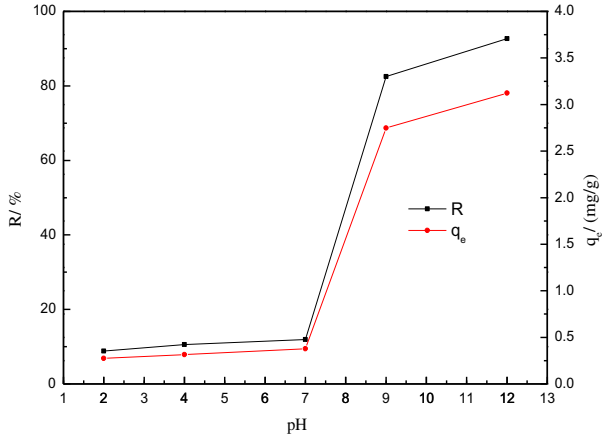

Fig. 10. The effect of pH on MB adsorption.

pseudo-first-order kinetic model

$$\ln(q_e - q_t) = \ln q_e - k_1 t \tag{3}$$

pseudo-second-order kinetic model

$$\frac{t}{q_t} = \frac{t}{q_e} + \frac{1}{k_2 q_e^2} \tag{4}$$

where k_1 (min^{-1}) and k_2 (g (mg min)$^{-1}$) are the rate constants of pseudo-first-order and pseudo-second-order, respectively. q_t (mg g^{-1}) and q_e (mg g^{-1}) are the adsorption capacities of MB at time t (min) and equilibrium, respectively. The kinetic parameters were determined from the intercepts and slopes of the fitted curves.

The kinetic data were fitted by the kinetic equations mentioned above, and the results are shown in Table 3. Based on the higher values of the coefficient ($R^2 > 0.994$), it can be affirmed that the adsorption kinetics of MB on ceramics were better described by the pseudo-second-order kinetic model, suggesting that the adsorption might be a chemisorption process [31,32].

Therefore, the rate constant k_2 can be applied to determine the apparent activation energy based on the Arrhenius equation:

$$\ln k_2 = \ln A - \frac{E_a}{RT} \tag{5}$$

where E_a (J mol^{-1}), R (8.314 J K^{-1} mol^{-1}), and T (K) are the apparent activation energy, the gas constant, and the absolute temperature, respectively. A is the pre-exponential factor (frequency factor).

The value of E_a was calculated to be 29.777 kJ mol^{-1} (Fig. 11). The value of the apparent activation energy cannot only respect the chemical

Table 3
The kinetic parameters for MB adsorption on EMR-based ceramics

Parameters		Pseudo-first-order kinetic model			Pseudo-second-order kinetic model		
T (℃)	c_0 (mg L^{-1})	q_e (mg g^{-1})	k_1 ($min^{-1} \times 10^{-3}$)	R^2	q_e (mg g^{-1})	k_2 ($min^{-1} \times 10^{-3}$)	R^2
30	50	0.825	5.9	0.972	1.103	5.431	0.994
40	50	1.362	9.6	0.972	1.569	8.319	0.999
50	50	1.817	12.8	0.982	2.381	11.28	0.999

reaction rate but can also give an idea about the type of adsorption. In general, a value of E_a lower than 4.184 kJ mol^{-1} corresponds to a physisorption process, whereas a value between 8.4 and 83.7 kJ mol^{-1} indicates that the adsorption process is chemisorption [33]. The value of E_a suggested that the adsorption was a chemisorption process.

3.6. Adsorption mechanism

To identify the importance of diffusion during the adsorption process of MB on EMR-based porous ceramics, the intraparticle diffusion model proposed by Weber and Morris was used to fit the kinetic data of MB adsorption, which is expressed as follows [34]:

$$q_t = k_i t^{1/2} + c_i \quad (6)$$

where k_i (mg g^{-1} $min^{-1/2}$) is the rate constant of the intraparticle diffusion model and c_i is the intercept related to the boundary layer effect [35]. The linearity of the plot ensured the intraparticle diffusion mechanism. The values of k_i and c_i can be evaluated from the slopes and intercepts of the plots of q_t vs. $t^{1/2}$

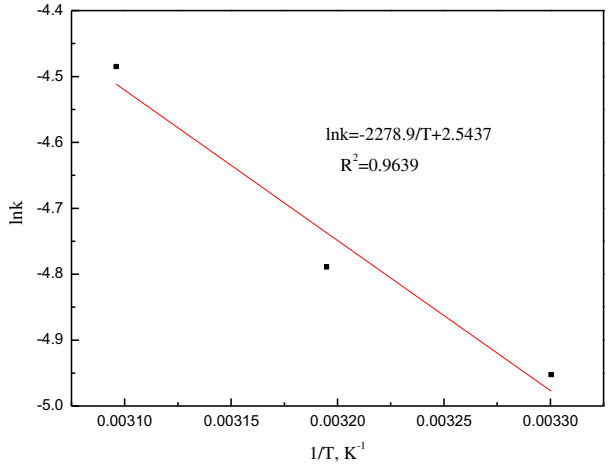

Fig. 11. Plot of ln k vs. $1/T$.

(Table 4). If the plots of q_t vs. $t^{1/2}$ are linear and pass through the origin, it means that the intraparticle diffusion is the sole rate-limiting step [36].

Fig. 12 shows that the plots were nonlinear for the whole range of the adsorption process, indicating that intraparticle diffusion was not the only rate-controlling step, but that other mechanisms such as the boundary layer may also influence the adsorption rate. Three distinguishable intercepting lines were clearly observed in Fig. 12, indicating that the adsorption of MB on EMR-based porous ceramics is a multi-step process, involving the diffusion of MB through the boundary layer to the surface of EMR-based porous ceramics, adsorption on the surface of EMR-based porous ceramics and intraparticle diffusion to the adsorption sites of EMR-based porous ceramics. Because the adsorption of MB at active sites of adsorbent was rapid, the rate of adsorption was mainly controlled by either intraparticle diffusion or boundary layer diffusion [37]. The first stage indicated rapid external surface adsorption or instantaneous adsorption because of the large surface area and the low competition between the MB molecules [38]. The second stage was attributed to the relatively slow adsorption. The plots of the second stage were linear, and the slopes k_i of plots of q_t vs. $t^{1/2}$ were lower compared to that of the first stage, reflecting the increase in the thickness of boundary layer and the decrease in the chance of external mass transfer, which can be attributed to the decreased concentration of MB at the second stage [38,39]. The last stage means that the adsorption and desorption on the EMR-based porous ceramics have finally reached equilibrium in which the adsorption isotherm is level and intraparticle diffusion starts to slow down. Furthermore, the plots at the three stages were linear, and none of the plots passed through the origin, indicating that the reaction rate was dually controlled by intraparticle diffusion and boundary layer diffusion throughout the adsorption process. The increase in the value of c_i with the adsorption progress implies that the influence of boundary layer diffusion on the adsorption process increases. Similar results were reported about the adsorption mechanism [40–42].

Table 4
The intraparticle diffusion model parameters for the adsorption of MB on EMR-based porous ceramics

Parameters		Intraparticle diffusion model					
		Stage 1		Stage 2		Stage 3	
T (℃)	c_0 (mg L^{-1})	k_i (mg g^{-1} $min^{-1/2}$)	R^2	k_i (mg g^{-1} $min^{-1/2}$)	R^2	k_i (mg g^{-1} $min^{-1/2}$)	R^2
30	50	0.0496	0.993	0.0359	0.993	0.0045	0.999
40	50	0.1099	0.997	0.0713	0.998	0.0123	0.994
50	50	0.1785	0.999	0.0889	0.996	0.0039	0.989

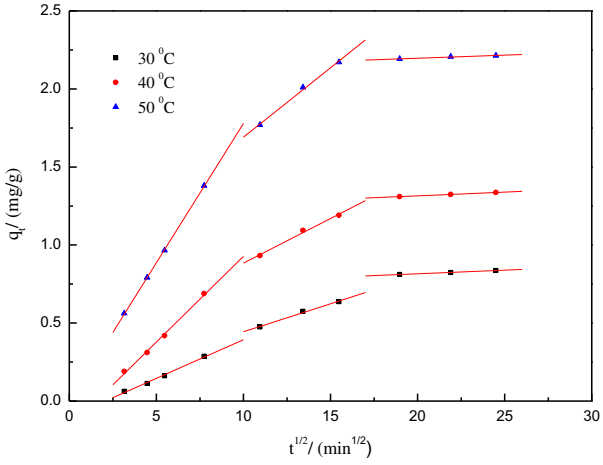

Fig. 12. Weber and Morris intraparticle diffusion plots for the removal of MB by EMR-based porous ceramics.

3.7. Equilibrium adsorption isotherm studies

For solid–liquid adsorption system, Langmuir and Freundlich isotherm models are widely used for describing the adsorption behavior.

The Langmuir isotherm model explains the monolayer adsorption onto a homogeneous surface with a finite number of identical sites [43]. The nonlinear form of the Langmuir isotherm model can be described by the following equation:

$$q_e = \frac{q_m k_L c_e}{1 + k_L c_e} \quad (7)$$

where k_L (L mg^{-1}) is the Langmuir adsorption coefficient. q_e (mg g^{-1}) and c_e (mg L^{-1}) are the adsorption capacity and the concentration of MB at equilibrium, respectively. q_m (mg g^{-1}) is the Langmuir maximum adsorption capacity.

The Freundlich isotherm model is an empirical equation that assumes that the adsorption occurs on a heterogeneous surface and the adsorption capacity of adsorbent increases infinitely with an increase in the initial concentration [44]. The nonlinear form of the Freundlich equation is commonly expressed as follows:

$$q_e = k_F c_e^{1/n} \quad (8)$$

where k_F ((mg g) (L $mg^{-1})^{1/n}$) is the Freundlich adsorption coefficient. $1/n$ is a characteristic constant and is related to adsorption intensity.

Fig. 13 shows the adsorption isotherms of MB on the EMR-based porous ceramics at different temperatures (30, 40 and 50 ℃) with an MB initial concentration range from 20 to 1,000 mg L^{-1}. The shape of the adsorption isotherm can largely provide information about the adsorption mechanism and can therefore be used to diagnose the nature of the adsorption [45]. It was obvious that the adsorption of MB on EMR-based porous ceramics was of the S1 type according to the Giles classification system of solid–solute adsorption (SSA) isotherms [46]. The results can be experimentally verified by the N_2 adsorption isotherm shown in Fig. 6.

Usually, in vapor or gas phase adsorption, the Langmuir isotherm model applies to the L-type adsorption isotherm, which is only confined to monolayer coverage taking into account forces between the adsorbate and the adsorbent, but the Freundlich isotherm model also allows for multi-layer coverage, which can be applied to the S-type adsorption isotherm [45]. On the basis of the characteristics of the equilibrium data and the shape of the adsorption isotherm, the Freundlich isotherm model was adopted to investigate the adsorption isotherm of MB on EMR-based porous ceramics, and the results are tabulated in Table 5 according to the equilibrium data shown in Fig. 13.

The good fit of the isotherm data to the Freundlich isotherm model indicates that the adsorption of MB occurred on the heterogeneous surface of the EMR-based porous ceramics. It was also clear that the values of k_F and n increased with increasing temperature, indicating that the adsorption became favorable at a higher temperature [47].

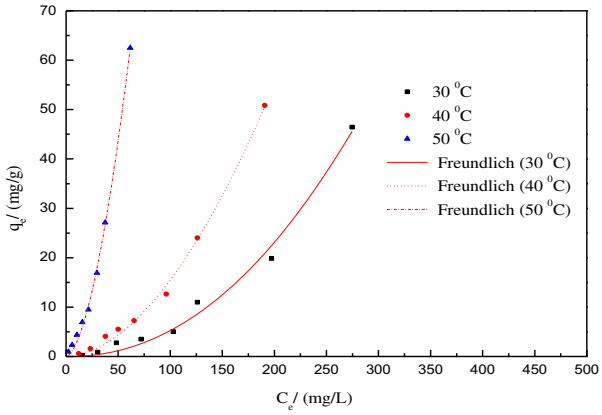

Fig. 13. Isotherm curves for the adsorption of MB on EMR-based porous ceramics.

Table 5
Equilibrium parameters for the adsorption of MB on EMR-based porous ceramics

	Freundlich isotherm		
T (℃)	k_F ((mg g) (L mg^{-1})$^{1/n}$ × 10^{-3})	n	R^2
30	0.27	0.466	0.991
40	3.35	0.546	0.997
50	54.03	0.584	0.998

3.8. Thermodynamics of adsorption

The adsorption process was evaluated by thermodynamic parameters such as the Gibbs free energy ΔG, enthalpy ΔH, and entropy ΔS. These parameters were calculated using the Gibbs equation and van't Hoff equation [48–51]:

$$\Delta G = -RT \ln(\rho K_D) \quad (9)$$

$$\Delta G = \Delta H - T \cdot \Delta S \quad (10)$$

where K_D ($K_D = q_e/c_e$, L g^{-1}) is the distribution coefficient. ρ (g L^{-1}) is the solution density. ΔG (kJ mol^{-1}) is the change in the Gibbs free energy. R (8.314 J (mol K)$^{-1}$) is the universal gas constant. T (K) is the temperature. ΔH (kJ mol^{-1}) and ΔS (J (mol K)$^{-1}$) are the values of the enthalpy change and entropy change, respectively. At a low concentration aqueous solution, the solution density is approximately equal to the water density (1,000 g L^{-1}), and the Gibbs equation can be simplified to the equation of T and K_D as follows:

$$\Delta G = -RT \ln K_D \quad (11)$$

The value of K_D for Eq. (11) was calculated from the corresponding q_e and c_e to a given c_e value at an initial MB concentration of 50 mg L^{-1}, and the value of q_e was obtained by the best-fitted isotherm equation (Eq. (8)) to a given c_e value [49–51]. The adsorption thermodynamic parameters for MB adsorption on the EMR-based porous ceramics are listed in Table 6. The negative values of ΔG and the positive value of ΔH suggest that the adsorption was a spontaneous and endothermic process. The absolute value of ΔH was higher than 40 kJ mol^{-1}, indicating that adsorption is a chemisorption process, which further confirms the correctness of this conclusion. The positive value of ΔS demonstrates the increased randomness at the solute/solid surface and the affinity of the EMR-based porous ceramics for MB adsorption.

3.9. Regeneration studies

The regeneration of adsorbent embodies an important factor for an advanced adsorbent from the viewpoint of environment protection and energy saving. Reuse experiments were carried out by placing the EMR-based porous ceramics after adsorption under the conditions of an initial concentration of 50 mg L^{-1} and 50℃ for 360 min into the furnace to roast at a temperature of 400℃ for 30 min. The recycling efficiency of EMR-based porous ceramics was investigated for the removal ratio of MB. As observed in Fig. 14, the removal ratios of MB were all higher than 92% after four cycles, indicating that compared to conventional activated carbon adsorbent, EMR-based porous ceramics have a great potential of being used as an MB adsorbent in industrial applications because

Table 6
Adsorption thermodynamic parameters for MB adsorption on the EMR-based porous ceramics

	ΔG				
Thermodynamic Parameters	30℃	40℃	50℃	ΔH	ΔS
Values	−6.57	−9.96	−14.10	107.64	376.53

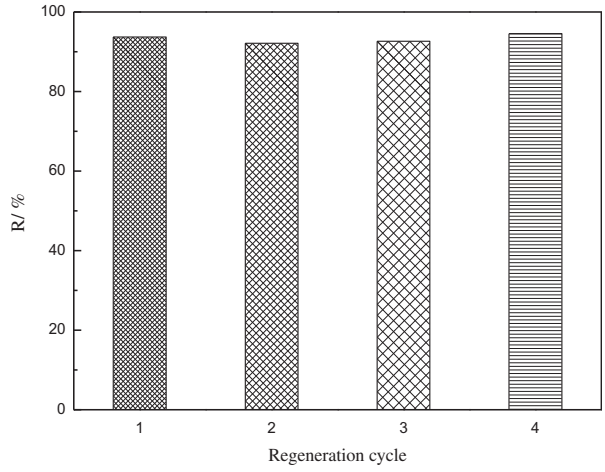

Fig. 14. The results of the regeneration experiments for the adsorption of MB on EMR-based porous ceramics.

they are economical, environmentally friendly, renewable and easy to produce.

4. Conclusions

In this work, EMR-based porous ceramics were prepared, characterized, and applied as an adsorbent for MB solution. Batch adsorption experiments showed that the MB adsorption was highly dependent on the contact time, temperature, initial concentration of MB, and pH. The MB adsorption kinetic and equilibrium data were analyzed using different kinetic and thermodynamic models. The results indicated that the pseudo-second-order kinetic model and the Freundlich isotherm model fit the experimental data well. The thermodynamic parameters indicated that the adsorption was a spontaneous, endothermic, and entropic-adding process. Conclusively, EMR-based porous ceramics are an economical, environmentally friendly, and high potential adsorbent for the removal of MB.

Acknowledgments

The authors would like to thank the National Natural Science Foundation of China (No. 21376273) and the National Science and Technology Support Program of China (No. 2015BAB17B01) for offering the research funds.

References

[1] K.R. Ramakrishna, T. Viraraghavan, Dye removal using low cost adsorbents, Water Sci. Technol. 36 (1997) 189–196.
[2] N. Panda, H. Sahoo, S. Mohapatra, Decolourization of Methyl Orange using Fenton-like mesoporous Fe_2O_3–SiO_2 composite, J. Hazard. Mater. 185 (2011) 359–365.
[3] A.F. Baybars, C. ozmetin, M. Korkmaz, Cationic dye (methylene blue) removal from aqueous solution by montmorillonite, Bull. Korean Chem. Soc. 33 (2012) 3184–3190
[4] C.X. Li, H. Zhong, S. Wang, J.R. Xue, Removal of basic dye (methylene blue) from aqueous solution using zeolite synthesized from electrolytic manganese residue, J. Ind. Eng. Chem. 23 (2015) 344–352.
[5] J. Zhang, Y. Zhou, M. Jiang, J. Li, J. Sheng, Removal of methylene blue from aqueous solution by adsorption on pyrophyllite, J. Mol. Liq. 209 (2015) 267–271.
[6] A. Houas, H. Lachheb, M. Ksibi, E. Elaloui, C. Guillard, J.M. Herrmann, Photocatalytic degradation pathway of methylene blue in water, Appl. Catal. B: Environ. 31 (2001) 145–157.
[7] V.S. Suvith, D. Philip, Catalytic degradation of methylene blue using biosynthesized gold and silver nanoparticles, Spectrochim. Acta Part A: Mol. Biomol. Spectrosc. 118 (2014) 526–532.
[8] H. Cherifi, B. Fatiha, H. Salah, Kinetic studies on the adsorption of methylene blue onto vegetal fiber activated carbons, Appl. Surf. Sci. 282 (2013) 52–59.
[9] S. Afroze, T.K. Sen, M. Ang, H. Nishioka, Adsorption of methylene blue dye from aqueous solution by novel biomass *Eucalyptus sheathiana* bark: Equilibrium, kinetics, thermodynamics and mechanism, Desalin. Water Treat. 57 (2015) 1–21.
[10] D. Ning, F. Wang, C.B. Zhou, C.L. Zhu, H.B. Yu, Analysis of pollution materials generated from electrolytic manganese industries in China, Resour. Conserv. Recycl. 54 (2010) 506–511.
[11] P. Szyczewski, J. Siepak, P. Niedzielski, T. Sobczyńskei, Research on heavy metals in Poland, Pol. J. Environ. Stud. 18 (2009) 755–768.
[12] T. Tsuru, Inorganic porous membranes for liquid phase separation, Sep. Purif. Rev. 30 (2001) 191–220.
[13] J. She, T. Ohji, Z.Y. Deng, Thermal shock behavior of porous silicon carbide ceramics, J. Am. Ceram. Soc. 85 (2002) 2125–2127.
[14] M.L. Dunn, M. Taya, Electromechanical properties of porous piezoelectric ceramics, J. Am. Ceram. Soc. 76 (1993) 1697–1706.
[15] C.P. Shaw, R.W. Whatmore, J.R. Alcock, Porous, functionally gradient pyroelectric materials, J. Am. Ceram. Soc. 90 (2007) 137–142.
[16] L. Yin, H.X. Peng, L. Yang, B. Su, Fabrication of three-dimensional inter-connective porous ceramics via ceramic green machining and bonding, J. Eur. Ceram. Soc. 28 (2008) 531–537.
[17] A.R. Walpole, Z. Xia, C.W. Wilson, J.T. Triffitt, P.R. Wilshaw, A novel nano-porous alumina biomaterial with potential for loading with bioactive materials, J. Biomed. Mater. Res. Part A 90A (2009) 46–54.
[18] X. Huang, Separator technologies for lithium-ion batteries, J. Solid State Electrochem. 15 (2011) 649–662.
[19] Z. Živcová, E. Gregorová, W. Pabst, Low-and high-temperature processes and mechanisms in the preparation of porous ceramics via starch consolidation casting, Starch-Stärke 62 (2010) 3–10.
[20] Z.K. Zhang, A. Li, Y.L. Yin, L. Zhao, Effect of crystallization time on behaviors of glass-ceramic produced

from sludge incineration ash, Procedia Environ. Sci. 18 (2013) 788–793.
[21] M. Erol, S. Küçükbayrak, A. Ersoy-Mericboyu, Production of glass-ceramics obtained from industrial wastes by means of controlled nucleation and crystallization, Chem. Eng. J. 132 (2007) 335–343.
[22] E. Ekrami, F. Dadashian, M. Arami, Adsorption of methylene blue by waste cotton activated carbon: Equilibrium, kinetics, and thermodynamic studies, Desalin. Water Treat. 57 (2015) 1–11.
[23] M. Vakili, M. Rafatullah, B. Salamatinia, A.Z. Abdullah, M.H. Ibrahim, K.B. Tan, Z. Gholami, P. Amouzgar, Application of chitosan and its derivatives as adsorbents for dye removal from water and wastewater: A review, Carbohydr. Polym. 113 (2014) 115–130.
[24] R.L. Burwell, Manual of symbols and terminology for physicochemical quantities and units—Appendix II: Heterogeneous catalysis, Pure Appl. Chem. 46 (1976) 71–90.
[25] K.S.W. Sing, Reporting physisorption data for gas/solid systems with special reference to the determination of surface area and porosity (Recommendations, 1984, Pure Appl. Chem. 57 (1985) 603–619.
[26] J.M. Salman, V.O. Njoku, B.H. Hameed, Batch and fixed-bed adsorption of 2,4-dichlorophenoxyacetic acid onto oil palm frond activated carbon, Chem. Eng. J. 174 (2011) 33–40.
[27] G.L. Dotto, M.L.G. Vieira, L.A.A. Pinto, Kinetics and mechanism of tartrazine adsorption onto chitin and chitosan, Ind. Eng. Chem. Res. 51 (2012) 6862–6868.
[28] R. Leyva-Ramos, L.E. Landin-Rodriguez, S. Leyva-Ramos, N.A. Medellin-Castillo, Modification of corncob with citric acid to enhance its capacity for adsorbing cadmium(II) from water solution, Chem. Eng. J. 180 (2012) 113–120.
[29] A. Benhouria, M.A. Islam, H. Zaghouane-Boudiaf, M. Boutahala, B.H. Hameed, Calcium alginate-bentonite-activated carbon composite beads as highly effective adsorbent for methylene blue, Chem. Eng. J. 270 (2015) 621–630.
[30] Y. Liu, Y. Kang, B. Mu, A.Q. Wang, Attapulgite/bentonite interactions for methylene blue adsorption characteristics from aqueous solution, Chem. Eng. J. 237 (2014) 403–410.
[31] Q. Qin, J. Ma, K. Liu, Adsorption of anionic dyes on ammonium-functionalized MCM-41, J. Hazard. Mater. 162 (2009) 133–139.
[32] S.D. Faust, O.M. Aly, Adsorption Processes for Water Treatment, Butterworth-Heinemann, Boston, MA, 1987.
[33] R.P. Han, J.J. Zhang, P. Han, Y.F. Wang, Z.H. Zhao, M.S. Tang, Study of equilibrium, kinetic and thermodynamic parameters about methylene blue adsorption onto natural zeolite, Chem. Eng. J. 145 (2009) 496–504.
[34] X. Han, W. Wang, X. Ma, Adsorption characteristics of methylene blue onto low cost biomass material lotus leaf, Chem. Eng. J. 171 (2011) 1–8.
[35] L. Wang, J. Zhang, R. Zhao, C. Li, Y. Li, C.L. Zhang, Adsorption of basic dyes on activated carbon prepared from Polygonum orientale Linn: Equilibrium, kinetic and thermodynamic studies, Desalination 254 (2010) 68–74.
[36] H.Y. Zhu, Y.Q. Fu, R. Jiang, J.H. Jiang, L. Xiao, G.M. Zeng, S.L. Zhao, Y. Wang, Adsorption removal of congo red onto magnetic cellulose/Fe_3O_4/activated carbon composite: Equilibrium, kinetic and thermodynamic studies, Chem. Eng. J. 173 (2011) 494–502.
[37] N. Kannan, K. Karuppasamy, Low cost adsorbents for the removal of phenylacetic acid from aqueous solution, Indian J. Environ. Prot. 18 (1998) 683–686.
[38] Y. Wang, W. Wang, A. Wang, Efficient adsorption of methylene blue on an alginate-based nanocomposite hydrogel enhanced by organo-illite/smectite clay, Chem. Eng. J. 228 (2013) 132–139.
[39] J. Ma, Y.Z. Jia, Y. Jing, Y. Yao, J.H. Sun, Kinetics and thermodynamics of methylene blue adsorption by cobalt-hectorite composite, Dyes Pigm. 93 (2012) 1441–1446.
[40] L.H. Ai, C.Y. Zhang, F. Liao, Y. Wang, M. Li, L.Y. Meng, J. Jiang, Removal of methylene blue from aqueous solution with magnetite loaded multi-wall carbon nanotube: Kinetic, isotherm and mechanism analysis, J. Hazard. Mater. 198 (2011) 282–290.
[41] Y.B. Liu, X.J. Gan, B.X. Zhou, B.T. Xiong, J.H. Li, C.P. Dong, J. Bai, W.M. Cai, Photoelectrocatalytic degradation of tetracycline by highly effective TiO_2 nanopore arrays electrode, J. Hazard. Mater. 171 (2009) 678–683.
[42] C.H. Weng, Y.T. Lin, T.W. Tzeng, Removal of methylene blue from aqueous solution by adsorption onto pineapple leaf powder, J. Hazard. Mater. 170 (2009) 417–424.
[43] I. Langmuir, The adsorption of gases on plane surfaces of glass, mica and platinum, J. Am. Chem. Soc. 40 (1918) 1361–1403.
[44] H.M.F. Freundlich, Uber die adsorption in lasugen (The adsorption behavior in solution systems), J. Phys. Chem. 57 (1906) 385–470.
[45] C.H. Giles, D. Smith, A. Huitson, A general treatment and classification of the solute adsorption isotherm. I. Theoretical. J. Colloid Interface Sci. 47 (1974) 755–765.
[46] C. Giles, T.H. MacEwan, S.N. Nakhwa, D. Smith, A system of classification of solution absorption isotherms, and its use in diagnosis of adsorption mechanisms and in measurement of specific surface areas of solids, J. Chem. Soc. (Resumed) 3 (1960) 3973–3993.
[47] Y.C. Sharma, Optimization of parameters for adsorption of methylene blue on a low-cost activated carbon, J. Chem. Eng. Data 55 (2009) 435–439.
[48] J. Zhang, D.Q. Cai, G.L. Zhang, C.J. Cai, C.L. Zhang, G.N. Qiu, K. Zheng, Z.Y. Wu, Adsorption of methylene blue from aqueous solution onto multiporous palygorskite modified by ion beam bombardment: Effect of contact time, temperature, pH and ionic strength, Appl. Clay Sci. 83–84 (2013) 137–143.
[49] S. Milonjic, A consideration of the correct calculation of thermodynamic parameters of adsorption, J. Serb. Chem. Soc. 72 (2007) 1363–1367.
[50] Y. Liu, Is the free energy change of adsorption correctly calculated? J. Chem. Eng. Data 54 (2009) 1981–1985.
[51] X.Y. Zhou, H.F. Liu, J.C. Hao, Letters to the editor: How to calculate the thermodynamic equilibrium constant using the langmuir equation, Adsorpt. Sci. Technol. 30 (2012) 647–650.